

# Direct Power Control of DFIG Wind Turbines with Super Capacitor Energy Storage Systems

Pindra Sattiraju<sup>1</sup>, Asst.Prof.G.Rajasekhar yadav<sup>2</sup>

<sup>1,2</sup>Department of Electrical and Electronics Engineering

<sup>1,2</sup>Avanathi Institute of Engineering & Technology, VSP

**Abstract-** Due to the price hike of the fossil fuels and the concern of the global warming, the development of wind power has rapidly progressed over the last decade. When wind turbines are connected to a grid, they should always maintain constant power. In order to maintain constant active power, the use of Doubly-Fed Induction Generators (DFIG) with Energy Storage System (ESS) like super capacitor (or) batteries can be used, with a two layer control scheme. In the two layers control there is a high-layer controller known as Wind Farm Supervisory Control (WFSC), which generates the active power ( $P$ ), Stator Power ( $P_s$ ), Energy storage power ( $P_e$ ), DC voltage ( $V_{dc}$ ) etc., references for the low-layer WTG controllers. The low-layer controller has two different controls i.e., Grid side controller (GSC) and Rotor side controller (RSC) which are used to control the AC/DC/AC converters of DFIG wind turbines and to generate the desired active power demand specified by the grid operator. Simulation is carried out in Matlab to evaluate the performance of wind farm equipped with 15 DFIG wind turbines with and without ESS to provide a constant active power of 36MW.

**Keywords-** Constant powers control (CPC), doubly fed induction generator (DFIG), energy storage, supervisory controller, wind turbine.

## I. INTRODUCTION

This paper proposes a novel two-layer constant power control (CPC) scheme for a wind farm equipped with doubly fed induction generator (DFIG) wind turbines [14], where each WTG is equipped with a super capacitor energy storage system (ESS). The CPC consists of a high-layer wind farm supervisory controller (WFSC) and low-layer WTG controllers. The high layer WFSC generates the active power references for the low layer WTG controllers of each DFIG wind turbine according to the active power demand from the grid operator. The low-layer WTG controllers then regulate each DFIG wind turbine to generate the desired amount of active power, where the deviations between the available wind energy input and desired active power output are compensated by the ESS. Simulation studies are carried out in PSCAD/EMTDC for a wind farm equipped with 15 DFIG

wind turbines to verify the effectiveness of the proposed control scheme.

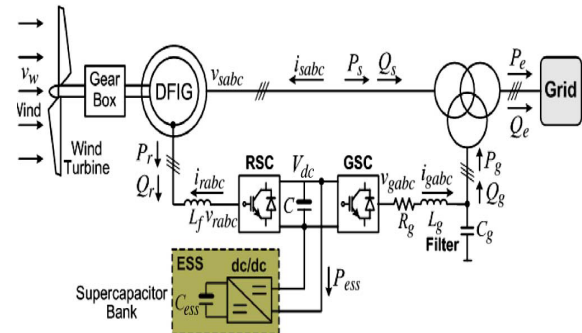


Figure 1. Configuration of a DFIG wind turbine equipped with a super capacitor ESS connected to a power grid

## II. DFIG WIND TURBINE WITH ENERGY STORAGE

Fig. 1 shows the basic configuration of a DFIG wind turbine equipped with a super capacitor-based ESS. The low speed wind turbine drives a high-speed DFIG through a gearbox. The DFIG is a wound-rotor induction machine. It is connected to the power grid at both stator and rotor terminals. The stator is directly connected to the grid, while the rotor is fed through a variable-frequency converter, which consists of a rotor-side converter (RSC) and a grid-side converter (GSC) connected back to back through a dc link and usually has a rating of a fraction (25%–30%) of the DFIG nominal power. As a consequence, the WTG can operate with the rotational speed in a range of  $\pm 25\%$ –30% around the synchronous speed, and its active and reactive powers can be controlled independently. In this paper, an ESS consisting of a super capacitor bank and a two-quadrant dc/dc converter is connected to the dc link of the DFIG converters. The ESS serves as either a source or a sink of active power and therefore contributes to control the generated active power of the WTG. The value of the capacitance of the super capacitor bank can be determined by

$$C_{ess} = \frac{P_n T}{V_{sc}^2} \quad (1)$$

where  $C_{ess}$  is in farads,  $P_n$  is the rated power of the DFIG in watts,  $V_{sc}$  is the rated voltage of the super capacitor bank in

volts, and T is the desired time period in seconds that the ESS can supply/store energy at the rated power (Pn) of the DFIG. The use of an ESS in each WTG rather than a large single central ESS for the entire wind farm is based on two reasons. First, this arrangement has a high reliability because the failure of a single ESS unit does not affect the ESS units in other WTGs. Second, the use of an ESS in each WTG can reinforce the dc bus of the DFIG converters during transients, thereby enhancing the low-voltage ride through capability of the WTG [10].

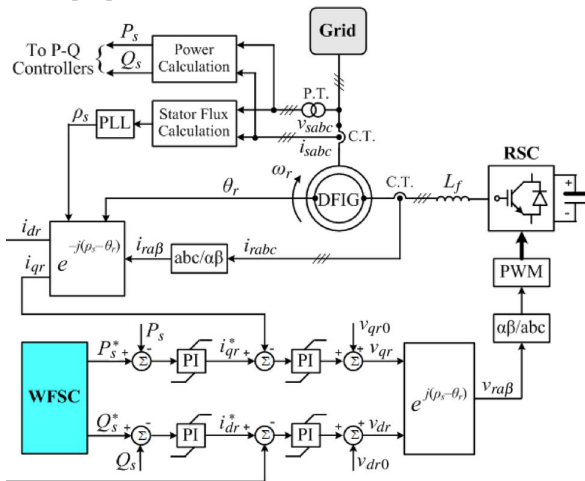


Figure 2. Overall vector control scheme of the RSC.

### III. CONTROL OF INDIVIDUAL DFIG WIND TURBINE

The control system of each individual DFIG wind turbine generally consists of two parts: 1) the electrical control of the DFIG and 2) the mechanical control of the wind turbine blade pitch angle [14], [15] and yaw system. Control of the DFIG is achieved by controlling the RSC, the GSC, and the ESS (see Fig. 1). The control objective of the RSC is to regulate the stator-side active power  $P_s$  and reactive power  $Q_s$  independently. The control objective of the GSC is to maintain the dc-link voltage  $V_{dc}$  constant and to regulate the reactive power  $Q_g$  that the GSC exchanges with the grid. In this paper, the mechanical control of the wind turbine blade pitch angle is similar.

#### A. Control of the RSC

Fig. 2 shows the overall vector control scheme of the RSC, in which the independent control of the stator active power  $P_s$  and reactive power  $Q_s$  is achieved by means of rotor current regulation in a stator-flux-oriented synchronously rotating reference frame [16]. Therefore, the overall RSC control scheme consists of two cascaded control loops. The outer control loop regulates the stator active and reactive

powers independently, which generates the reference signals  $i^*_{dr}$  and  $i^*_{qr}$  of the d- and q-axis current components, respectively, for the inner-loop current regulation. The outputs of the two current controllers are compensated by the corresponding cross-coupling terms  $v_{dr0}$  and  $v_{qr0}$  [14], respectively, to form the total voltage signals  $v_{dr}$  and  $v_{qr}$ . They are then used by the pulse width modulation (PWM) module to generate the gate control signals to drive the RSC. The reference signals of the outer-loop power controllers are generated by the high-layer WFSC

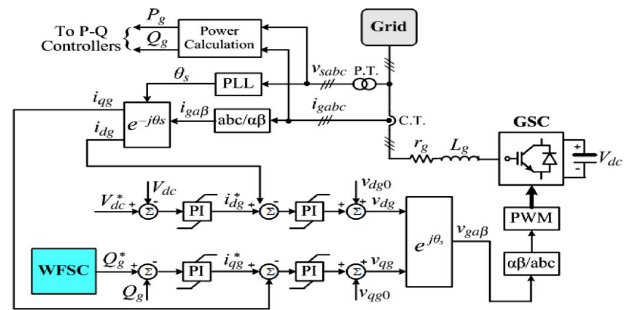


Figure 3. Overall vector control scheme of the GSC.

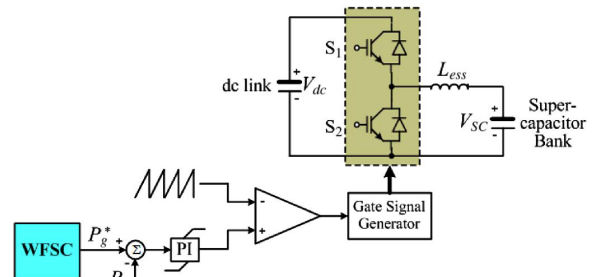


Figure 4. Configuration and control of the ESS.

#### B. Control of the GSC

Fig. 3 shows the overall vector control scheme of the GSC, in which the control of the dc-link voltage  $V_{dc}$  and the reactive power  $Q_g$  exchanged between the GSC and the grid is achieved by means of current regulation in a synchronously rotating reference frame [16]. Again, the overall GSC control scheme consists of two cascaded control loops. The outer control loop regulates the dc-link voltage  $V_{dc}$  and the reactive power  $Q_g$ , respectively, which generates the reference signals  $i^*_{dg}$  and  $i^*_{qg}$  of the d- and q-axis current components, respectively, for the inner-loop current regulation. The outputs of the two current controllers are compensated by the corresponding cross coupling terms  $v_{dg0}$  and  $v_{qg0}$  [14], respectively, to form the total voltage signals  $v_{dg}$  and  $v_{qg}$ . They are then used by the PWM module to generate the gate control signals to drive the GSC. The reference signal of the outer-loop reactive power controller is generated by the high-layer WFSC.

**C. Configuration and Control of the ESS**

Fig. 4 shows the configuration and control of the ESS. The ESS consists of a super capacitor bank and a two-quadrant dc/dc converter connected to the dc link of the DFIG. The dc/dc converter contains two insulated-gate bipolar transistor (IGBT) switches S1 and S2. Their duty ratios are controlled to regulate the active power  $P_g$  that the GSC exchanges with the grid. In this configuration, the dc/dc converter can operate in two different modes, i.e., buck or boost mode, depending on the status of the two IGBT switches. If S1 is open, the dc/dc converter operates in the boost mode; if S2 is open, the dc/dc converter operates in the buck mode. The duty ratio D1 of S1 in the buck mode can be approximately expressed as

$$D_1 = \frac{V_{sc}}{V_{dc}} \tag{2}$$

and the duty ratio D2 of S2 in the boost mode is  $D_2 = 1 - D_1$ . In this paper, the nominal dc voltage ratio  $V_{SC,n}/V_{dc,n}$  is 0.5, where  $V_{SC,n}$  and  $V_{dc,n}$  are the nominal voltages of the super capacitor bank and the DFIG dc link, respectively. Therefore, the nominal duty ratio D1,n of S1 is 0.5.

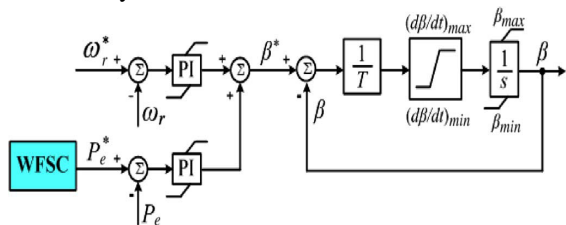


Figure 5. Blade pitch control for the wind turbine.

The operating modes and duty ratios D1 and D2 of the dc/dc converter are controlled depending on the relationship between the active powers  $P_r$  of the RSC and  $P_g$  of the GSC. If  $P_r$  is greater than  $P_g$ , the converter is in buck mode and D1 is controlled, such that the super capacitor bank serves as a sink to absorb active power, which results in the increase of its voltage VSC. On the contrary, if  $P_g$  is greater than  $P_r$ , the converter is in boost mode and D2 is controlled, such that the super capacitor bank serves as a source to supply active power, which results in the decrease of its voltage VSC. Therefore, by controlling the operating modes and duty ratios of the dc/dc converter, the ESS serves as either a source or a sink of active power to control the generated active power of the WTG. In Fig. 4, the reference signal  $P^*_g$  is generated by the high-layer WFSC.

**D. Wind Turbine Blade Pitch Control**

Fig. 5 shows the blade pitch control for the wind turbine, where  $\omega_r$  and  $P_e (= P_s + P_g)$  are the rotating speed and output

active power of the DFIG, respectively. When the wind speed is below the rated value and the WTG is required to generate the maximum power,  $\omega_r$  and  $P_e$  are set at their reference values, and the blade pitch control is deactivated. When the wind speed is below the rated value, but the WTG is required to generate a constant power less than the maximum power, the active power controller may be activated, where the reference signal  $P^*_e$  is generated by the high-layer WFSC and  $P_e$  takes the actual measured value. The active power controller adjusts the blade pitch angle to reduce the mechanical power that the turbine extracts from wind. This reduces the imbalance between the turbine mechanical power and the DFIG output active power, thereby reducing the mechanical stress in the WTG and stabilizing the WTG system. Finally, when the wind speed increases above the rated value, both  $\omega_r$  and  $P_e$  take the actual measured values, and both the speed and active power controllers are activated to adjust the blade pitch angle.

Flow Chart Implementation:

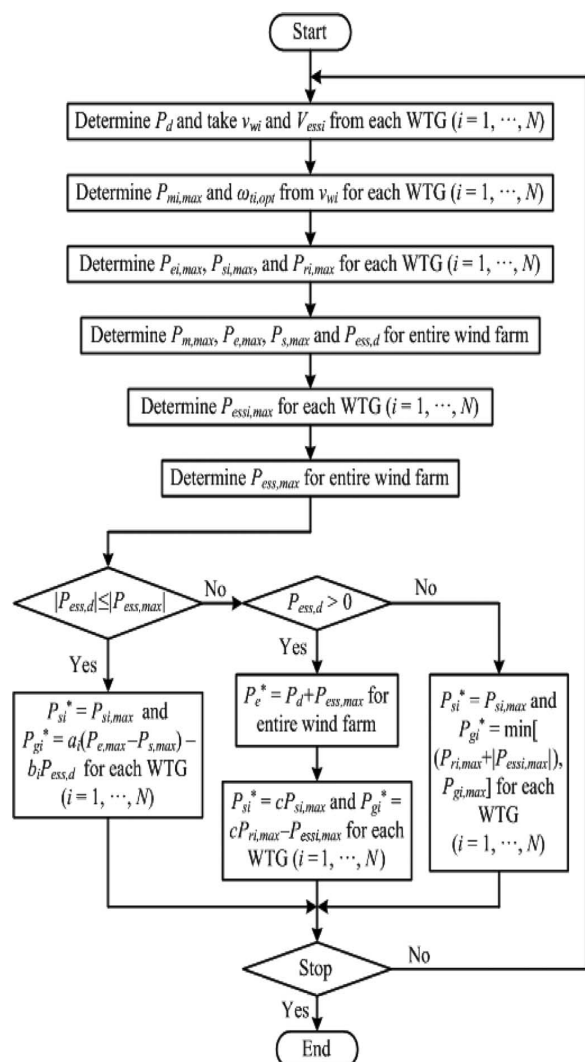


Figure 6. Flowchart of implementation of the WFSC.

can be determined, which is proportional to the wind speed  $v_{wi}$  at a certain pitch angle  $\beta_i$

$$\omega_{ti,opt} = k(\beta_i)v_{wi} \quad (3)$$

where  $k$  is a constant at a certain value of  $\beta_i$ . Then, the maximum mechanical power  $P_{mi,max}$  that the wind turbine extracts from the wind can be calculated by the well-known wind turbine aerodynamic characteristics

$$P_{mi,max} = \frac{1}{2} \rho_i A_r v_{wi}^3 C_{Pi}(\lambda_{i,opt}, \beta_i) \quad (4)$$

where  $\rho_i$  is the air density in kilograms per cubic meter;  $A_r = \pi R^2$  is the area in square meters swept by the rotor blades with  $R$  being the blade length in meters; and  $C_{Pi}$  is the power coefficient, which is a function of both tip-speed ratio  $\lambda_i$  and the blade pitch angle  $\beta_i$ , where  $\lambda_i$  is defined by

$$\lambda_i = \frac{\omega_{ti} R}{v_{wi}} \quad (5)$$

In (4),  $\lambda_{i,opt}$  is the optimal tip-speed ratio when the wind turbine rotates with the optimal speed  $\omega_{ti,opt}$  at the wind speed  $v_{wi}$ .

Given  $P_{mi,max}$ , the maximum active power  $P_{ei,max}$  generated by the WTG can be estimated by taking into account the power losses of the WTG [14]

$$P_{ei,max} = P_{mi,max} - P_{Li} = P_{si,max} + P_{ri,max} \quad (6)$$

where  $P_{Li}$  is the total power losses of WTG  $i$ , which can be estimated by the method in [14];  $P_{si,max}$  and  $P_{ri,max}$  are the maximum DFIG stator and rotor active powers of WTG  $i$ , respectively. In terms of the instantaneous variables in Fig. 1, the stator active power  $P_s$  can be written in a synchronously rotating dq reference frame [16] as follows:

$$P_s = \frac{3}{2} (v_{ds} i_{ds} + v_{qs} i_{qs}) \approx \frac{3}{2} [\omega_s L_m (i_{qs} i_{dr} - i_{ds} i_{qr}) + r_s (i_{ds}^2 + i_{qs}^2)] \quad (7)$$

where  $v_{ds}$  and  $v_{qs}$  are the d- and q-axis voltage components of the stator windings, respectively;  $i_{ds}$  and  $i_{qs}$  are the stator d- and q-axis current components, respectively;  $i_{dr}$  and  $i_{qr}$  are the rotor d- and q-axis current components, respectively;  $\omega_s$  is the rotational speed of the synchronous reference frame; and  $r_s$  and  $L_m$  are the stator resistance and mutual inductance, respectively. Similarly, the rotor active power is calculated by

$$P_r = \frac{3}{2} (v_{dr} i_{dr} + v_{qr} i_{qr}) \approx \frac{3}{2} [-s \omega_s L_m (i_{qs} i_{dr} - i_{ds} i_{qr}) + r_r (i_{dr}^2 + i_{qr}^2)] \quad (8)$$

where  $v_{dr}$  and  $v_{qr}$  are the d- and q-axis voltage components of the rotor windings, respectively;  $s$  is the slip of the DFIG defined by

$$s = (\omega_s - \omega_r) / \omega_s \quad (9)$$

where  $\omega_r$  is the DFIG rotor speed. (7) and (8) yield

$$P_r = -\frac{P_s - 3i_{ds}^2 r_s}{P_s - 3i_{qs}^2 r_s} \quad (10)$$

Where  $i_s = \sqrt{i_{ds}^2 + i_{qs}^2} / 2$  and  $i_r = \sqrt{i_{dr}^2 + i_{qr}^2} / 2$ . If neglecting the stator copper loss  $3i_{ds}^2 r_s$  and rotor copper loss  $3i_{dr}^2 r_r$  of the DFIG, the relationship between the stator and rotor active powers can be approximated by

$$P_r = -s P_s \quad (11)$$

According to (6) and (10) [or (11)],  $P_{si,max}$  and  $P_{ri,max}$  of each WTG can be determined. Then, the total maximum mechanical power  $P_{m,max}$ , DFIG output active power  $P_{e,max}$ , and stator active power  $P_{s,max}$  of all WTGs in the wind farm can be calculated as

$$P_{mi,max} = \sum_{i=1}^N P_{mi,max} \quad (12)$$

$$P_{ei,max} = \sum_{i=1}^N P_{ei,max} \quad (13)$$

$$P_{s,max} = \sum_{i=1}^N P_{s,max} \quad (14)$$

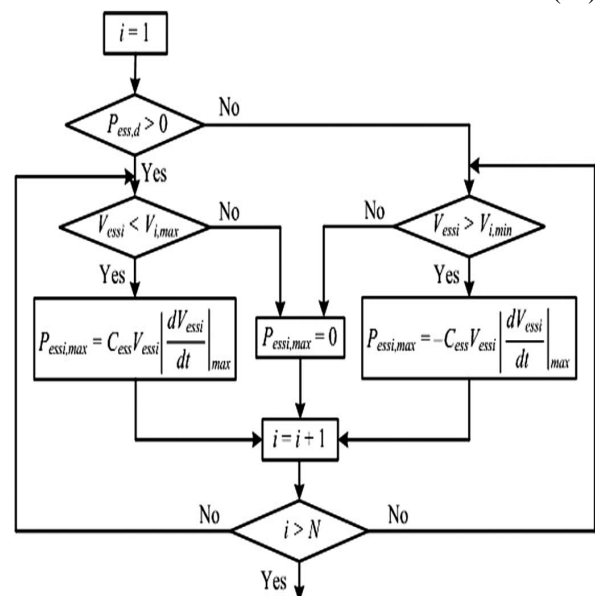


Figure 7. Flowchart of determination of  $P_{essi,max}$  for each WTG.

In order to supply constant power  $P_d$  to the grid, the deviation  $P_{ess,d}$  between the demand/commitment  $P_d$  and the maximum generation  $P_{e,max}$  is the power that should be stored in or supplied from the ESSs of the WTGs

$$P_{ess,d} = P_{e,max} - P_d \tag{15}$$

On the other hand, the capability of each ESS to store or supply power depends on the capacitance  $C_{ess}$  and the voltage  $V_{essi}$  of the supercapacitor bank. During normal operation,  $V_{essi}$  must be maintained within the following range:

$$V_{i,min} < V_{essi} < V_{i,max} \tag{16}$$

where  $V_{i,max}$  and  $V_{i,min}$  are the maximum and minimum operating voltages of the supercapacitor bank, respectively. The maximum power  $P_{essi,max}$  that can be exchanged between the supercapacitor bank and the DFIG dc link of WTG  $i$  can be determined by

$$P_{essi,max} = \pm C_{ess} V_{essi} \left| \frac{dV_{essi}}{dt} \right|_{max} \tag{17}$$

where  $|dV_{essi}/dt|_{max}$  is the maximum rate of voltage variations of the supercapacitor bank, which is related to the current limits of the supercapacitor bank. In (17), the positive sign indicates storing energy, while the negative sign indicates supplying energy by the ESS. The calculation of  $P_{essi,max}$  for each WTG is subjected to (16). Fig. 7 shows how to determine  $P_{essi,max}$  for each WTG. If  $P_{ess,d} > 0$ , extra power needs to be stored in the ESSs. In this case, if  $V_{essi} < V_{i,max}$ ,  $P_{essi,max}$  is calculated by (17) and takes the positive sign; otherwise, the ESS cannot store any power and  $P_{essi,max} = 0$ . On the contrary, if  $P_{ess,d} < 0$ , active power needs to be supplied from the ESSs. In this case, if  $V_{essi} > V_{i,min}$ ,  $P_{essi,max}$  is calculated by (17) and takes the negative sign; otherwise, the ESS cannot supply any power and  $P_{essi,max} = 0$ .

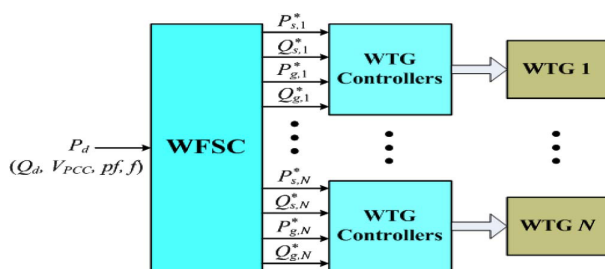


Figure 8. Proposed two-layer CPC scheme for the wind farm.

#### IV. SIMULATION RESULTS

Simulation studies are carried out for a wind farm with 15 DFIG wind turbines (see Fig. 9) to verify the

effectiveness of the proposed control scheme under various operating conditions. Each DFIG wind turbine (see Fig. 1) has a 3.6-MW power capacity [14], [15]. The total power capacity of the wind farm is 54 MW. Each DFIG wind turbine is connected to the internal network of the wind farm through a 4.16/34.5-kV voltage step-up transformer. The high-voltage terminals of all transformers in the wind farm are connected by 34.5-kV power cables to form the internal network of the wind farm. The entire wind farm is connected to the utility power grid through a 34.5/138-kV voltage step-up transformer at PCC to supply active and reactive powers of  $P$  and  $Q$ , respectively. In this paper, the power grid is represented by an infinite source. The ESS of each WTG is designed to continuously supply/store 20% of the DFIG rated power for approximately 60 s. Then, the total capacitance of the super capacitor bank can be obtained from (1). The parameters of the WTG, the ESS, and the power network are listed in the Appendix. Some typical results are shown and discussed in this section.

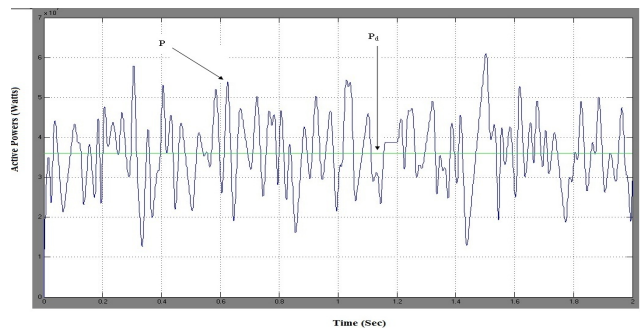


Figure 9. shows the total active power

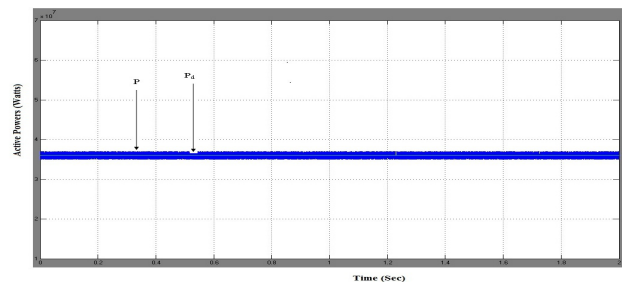


Figure 10. Total power of wind farm

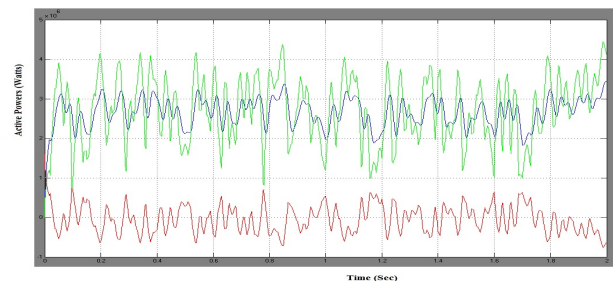


Figure 11. shows the stator power ( $P_{s1}$ ), and the GSC active power ( $P_{g1}$ ) of WTG 1

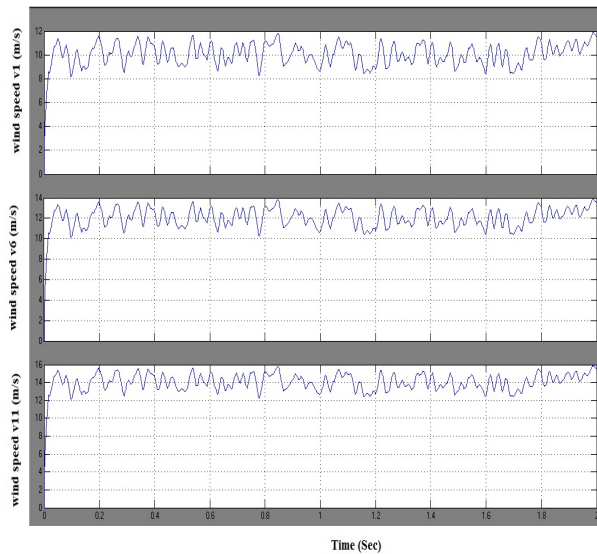


Figure 12. shows the variations of wind speeds provided to the Doubly-Fed Induction Generator WTG1, WTG6 and WTG11

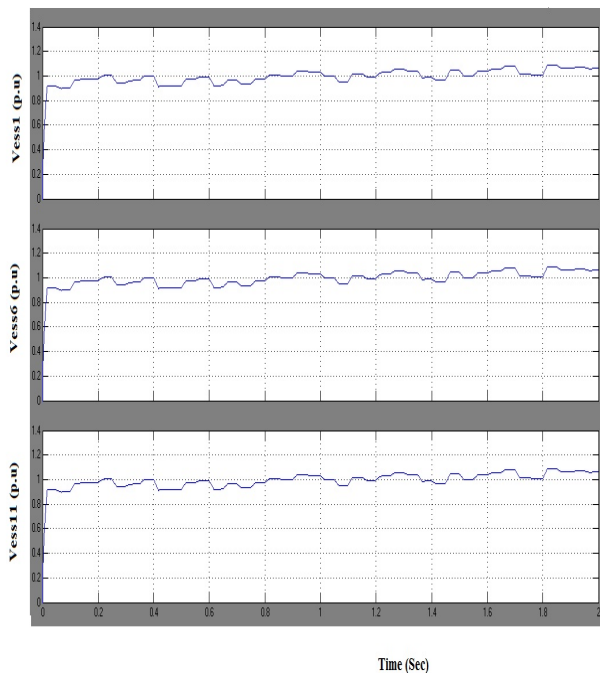


Figure 13. shows the voltages of the super capacitor banks of WTG1, WTG6, and WTG11.

## V. CONCLUSION

In the present work, the design of a wind farm is done using 15 DFIG's each producing 3.6MW power. The proposed control strategies for controlling the rotor and grid side converters are also described. The simulation is done with a 120kv grid which supplies a constant power of 36MW which is connected to the wind farm. Simulation results are observed for the power supplied by the wind farm with and without ESS, here observation has been made that without ESS the

total power generated by wind farm has high variations compared to the wind farm with ESS where we can observe a constant active power is obtained. With step changes in power at the grid, the power tracking performance of the wind farm generates active power by the wind farm dynamically by tracking the power demand with good precision. This power tracking capability cannot be achieved without using the ESSs or the proposed control scheme. The proposed system and control schemes provides a promising solution to help achieve high levels of penetration of wind power into electric power grids.

## REFERENCES

- [1] "Focus on 2030: EWEA aims for 22% of Europe's electricity by 2030," Wind Directions, pp. 25–34, Nov./Dec. 2006.
- [2] 20% Wind Energy By 2030: Increasing Wind Energy's Contribution to U.S. Electricity Supply, U.S. Department of Energy, Jul. 2008.
- [3] W. Qiao and R. G. Harley, "Grid connection requirements and solutions for DFIG wind turbines," in Proc. IEEE Energy Conf., Atlanta, GA, Nov. 17–18, 2008, pp. 1–8.
- [4] Wind Generation & Total Load in the BPA Balancing Authority: DOE Bonneville Power Administration, U.S. Department of Energy. [Online]. Available: <http://www.transmission.bpa.gov/business/operations/Wind/default.aspx>
- [5] R. Piwko, D. Osborn, R. Gramlich, G. Jordan, D. Hawkins, and K. Porter, "Wind energy delivery issues: Transmission planning and competitive electricity market operation," IEEE Power Energy Mag., vol. 3, no. 6, pp. 47–56, Nov./Dec. 2005.
- [6] L. Landberg, G. Giebel, H. A. Nielsen, T. Nielsen, and H. Madsen, "Shortterm prediction—An overview," Wind Energy, vol. 6, no. 3, pp. 273–280, Jul./Sep. 2003.
- [7] M. Milligan, B. Kirby, R. Gramlich, and M. Goggin, Impact of Electric Industry Structure on High Wind Penetration Potential, Nat. Renewable Energy Lab., Golden, CO, Tech. Rep. NREL/TP-550-46273. [Online]. Available: <http://www.nrel.gov/docs/fy09osti/46273.pdf>
- [8] J. P. Barton and D. G. Infield, "Energy storage and its use with intermittent renewable energy," IEEE Trans. Energy Convers., vol. 19, no. 2, pp. 441–448, Jun. 2004.

- [9] D. Rastler, "Electric energy storage, an essential asset to the electric enterprise: Barriers and RD&D needs," California Energy Commission Staff Workshop Energy Storage Technol., Policies Needed Support California's RPS Goals 2020, Sacramento, CA, Apr. 2, 2009.
- [10] C. Abbey and G. Joos, "Supercapacitor energy storage for wind energy applications," *IEEE Trans. Ind. Appl.*, vol. 43, no. 3, pp. 769–776, May/Jun. 2007.
- [11] B. S. Borowy and Z. M. Salameh, "Dynamic response of a stand-alone wind energy conversion system with battery energy storage to wind gust," *IEEE Trans. Energy Convers.*, vol. 12, no. 1, pp. 73–78, Mar. 1997.
- [12] M.-S. Lu, C.-L. Chang, W.-J. Lee, and L. Wang, "Combining the wind power generation system with energy storage equipments," *IEEE Trans. Ind. Appl.*, vol. 45, no. 6, pp. 2109–2115, Nov./Dec. 2009.
- [13] A. Yazdani, "Islanded operation of a doubly-fed induction generator (DFIG) wind-power system with integrated energy storage," in *Proc. IEEE Canada Elect. Power Conf.*, Montreal, QC, Canada, Oct. 25–26, 2007, pp. 153–159.
- [14] W. Qiao, W. Zhou, J. M. Aller, and R. G. Harley, "Wind speed estimation based sensorless output maximization control for a wind turbine driving a DFIG," *IEEE Trans. Power Electron.*, vol. 23, no. 3, pp. 1156–1169, May 2008.
- [15] W. Qiao, G. K. Venayagamoorthy, and R. G. Harley, "Real-time implementation of a STATCOM on a wind farm equipped with doubly fed induction generators," *IEEE Trans. Ind. Appl.*, vol. 45, no. 1, pp. 98–107, Jan./Feb. 2009.
- [16] D. W. Novotny and T. A. Lipo, *Vector Control and Dynamics of AC Drives*. Oxford, U.K.: Oxford Univ. Press, 2000.